Microwave Characterization and Modeling of the Surface Impedance of Fractal Structure Copper Films

Emmanuel Troncet, Guy Ablart, and Levi Allam

***Abstract*—The surface impedances Zs of two thin metallic films of different fractal structures realized on printed circuits have been measured in free-space over the frequency range [10 GHz, 20 GHz]. A modeling scheme based on Maxwell's equations and Fresnel's diffraction theory is proposed.**

***Index Terms*—Fractals, impedance measurement, thin films.**

I. Introduction

A MATERIAL of fractal structure is a highly disordered set, presenting irregularities at all scales of observation. The concept of fractal geometry, indispensable complement to the Euclidean geometry, permits a description of a symmetry of expansion. This notion is closely related to the scale-invariance properties to which is associated the fractal dimension number characterizing the fractal material's morphology [1]–[3]. Such structures present a special interest regarding their possible properties of absorbing electromagnetic waves.

The present study is composed of three parts. First, we give the realization procedure of two samples of known fractal dimensions. Their parameters and the roles of each of them will be presented. In the course of the second part, a detailed description of the measure test bench in free-space is presented along with an explanation of technical options that we were required to adopt. Therefore, in order to point out the properties of absorbing electromagnetic waves, experimental investigations on surface impedance of our samples have been done over the frequency range [10 GHz, 20 GHz]. Surface impedance is composed of a real part (or resistance), which is responsible of conduction losses, and an imaginary part (or reactance), which translates the depth of wave penetration in the material. Finally, in the third part, we propose a modeling scheme of the physical behavior of two fractal structures samples. For this it is necessary to investigate locally the propagation across the material of a rectilinearly plane-polarized wave (RPPW) and then to generalize the phenomenon to the entire surface under consideration.

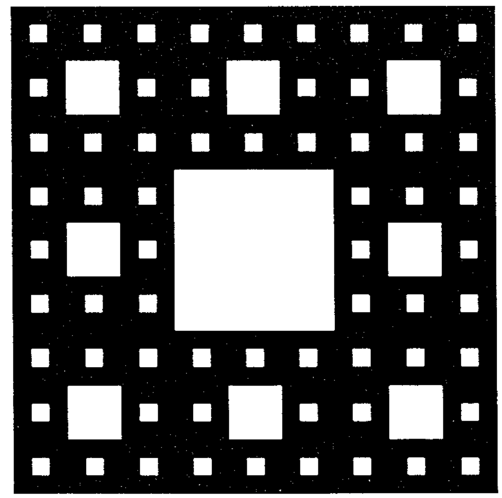

Fig. 1. Sierpinski carpet.

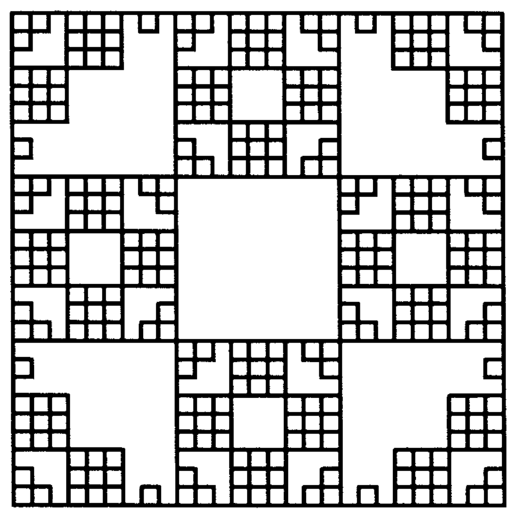

Fig. 2. Curve of Von Koch.

II. Realization of Two Fractal Structure Samples

In order to meet the necessities of the measure test bench in free-space, we have designed each of the two samples on a dielectric support according to the technique commonly employed in printed circuits, choosing sufficiently big formats:

- 10 cm $\times$ 10 cm for the fractal structures;
- 30 cm $\times$ 30 cm for epoxy supports.

We can, as such, design exactly the type of structure we wish study to the chosen dimensions but limited by technical contraints all the same. The two motifs of fractal nature we have realized are the Sierpinski carpet and a curve of Von Koch (Figs. 1 and 2).

Manuscript received October 18, 1996; revised June 9, 1997.

E. Troncet and G. Ablart are with L.M.E.Q. Université Paul Sabatier, Toulouse, 31062, Cedex 04 France.

L. Allam is with the Université d'Orléans, IUT de Chartres, 1 place Mendès France, Chartres, 28000 France.

Publisher Item Identifier S 0018-926X(98)02270-4.

TABLE I
PARAMETERS OF THE SYSTEM

	Air	Copper	Substrate
Conductivity (S/m)	nil	$\sigma_1 = 5.81\ 10^7$	nil
Permittivity (F/m)	$\varepsilon_0 = 8.85\ 10^{-12}$	$\varepsilon_1 = \varepsilon_0$	$\varepsilon_2 = 2.33\varepsilon_0$
Permeability (H/m)	$\mu_0 = 4\pi\ 10^{-7}$	$\mu_1 = \mu_0$	$\mu_2 = \mu_0$
Thickness (μm)	—	35	1600

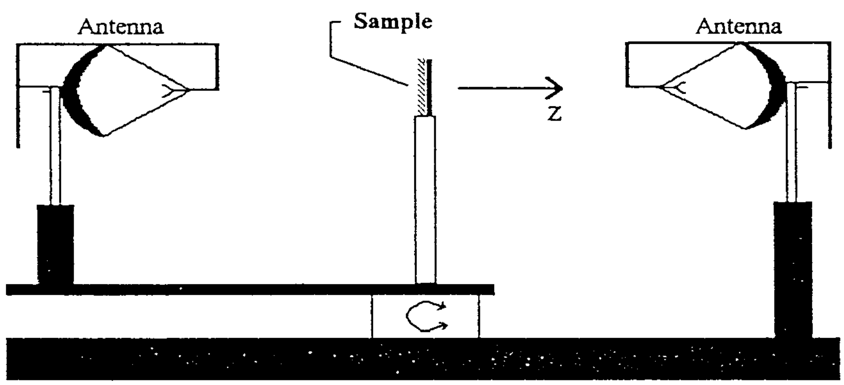

Fig. 3. Measure test bench.

In spite of the apparent complexity of these structures, it's easy to notice their self similarity [1]. The associated fractal dimensions are $D = 1.89$ for the Sierpinski carpet and $D = 1.5$ for the curve of Koch. The two samples have been elaborated to the fourth-order iteration. It's necessary to note that the printed circuit method does not allow a high number of iterations because of a limited resolution. The considered parameters for the copper and the substrate are recalled in Table I.

III. Microwave Characterization

A. Description of the Measure Test Bench

For our measurements, we have used the test bench of Baccarat of the CERT [4]. Its principal constituents are two antennas (one for transmission, the other for reception), an analyzer HP8720, and an acquisition system. The principle of this measure test bench is shown schematically in Fig. 3.

The sample that will be characterized is placed on the axis between the two antennas and positioned with an angular precision of 0.05° and 0.01 mm in distance. The receiving antenna is fixed while the emission antenna is mounted on a rotating support, which permits the measurements either in bistatic or with variable incidences. In addition, one of the antennas is adjustable in such a way that the measurements can be made in parallel as well as perpendicular polarization.

For a correct functioning of the system, it is advisable to free the sample under test from the external environment. For this the test bench has at its disposal two complementary methods: a temporal filtration of the response and a system of focussing the wave.

The temporal filtration permits the elimination of strays and, thus, improve the quality of the signal. The principle is based on the Fourier transform of the signal, which provides the temporal response. Then, this response is filtered in a manner to keep only the part corresponding to the reflection of the wave on the material. Thereafter, the inverse Fourier transform gives back the frequency response. The choice of a finite frequency band (called the observation window) is very important in order not to depreciate the response. This choice is made experimentally by trial and error.

The system of focusing the wave presents the advantage of rendering negligible the effect of diffraction on the edges of the sample. In fact, the energy remains concentrated at the center of the sample and, thus, reaches less on its sides. The two ellipsoidal confocal antennas have at their first focus a horn obeying Gaussian illumination law. This device generates a Gaussian beam between the two reflectors, which display a plane wave structure at the sample level (centered system). The electromagnetic plane waves are transverse waves perpendicular to the direction of propagation.

The depth of the measure test bench field is 5λ, where λ is the wavelength. It characterizes the distance, following the z axis around the focal plane on which the wavefront can be considered as plane. This distance is quite suitable for our two samples made of thin metallic films ($5\lambda = 10$ cm at 15 GHz). In order to neglect the effects of diffraction on the edges, it is necessary to be provided with a sample whose dimensions reach at least 6 $\lambda \times 6\lambda$. The design formats cited above satisfy these conditions. A calibration of the measuring channel permits to initialize the reflection of a thick metallic plate (perfect reflector) at one and this under experimental conditions. The frequency range is from 9.6 to 18.4 GHz with a resolution of 0.011 GHz.

The surface impedance of the object is not directly accessible, but is deduced from the measurement of the reflection coefficient S_{11} (amplitude in decibels and phase in degrees) by the following relationship:

$$Zs = 120\pi \frac{1 - S_{11}}{1 + S_{11}}. \tag{1}$$

The parameter S_{11} is obtained using an analyzer that compares the wave transmitted to the receiving antenna with the incident wave. The main advantage of this technique is the total absence of contact with the material.

B. Experimental Results

The Figs. 4(a) and 5(a) show the evolution of the surface impedance of each of the two samples as a function of the frequency. An enlargement of the frequency scale [Figs. 4(b) and 5(b)] permits a more precise view of the surface impedance behavior, which recurs all over the range. Each time the real part Rs is distinguished from the imaginary part Xs.

In both cases, a relatively complex frequency behavior is noticed. On each curve, one can observe multiple oscillations of different frequencies which are superimposed. Each of the two resistances Rs varies around an average value (approximately 55 Ω for Sierpinski carpet and 90 Ω for the Koch's curve), which is as much higher as the copper content is lower in the structure. Indeed, at the limit it must tend toward the characteristic impedance of the vacuum, i.e., 377 Ω.

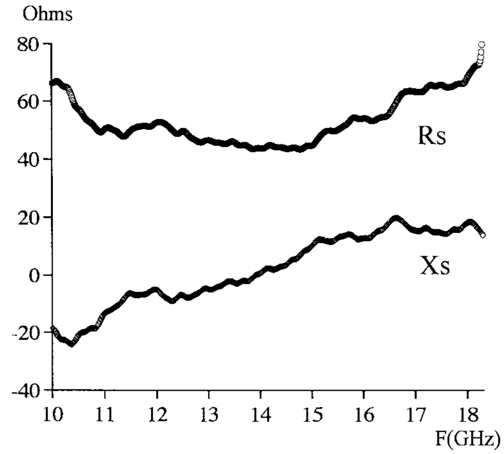

(a)

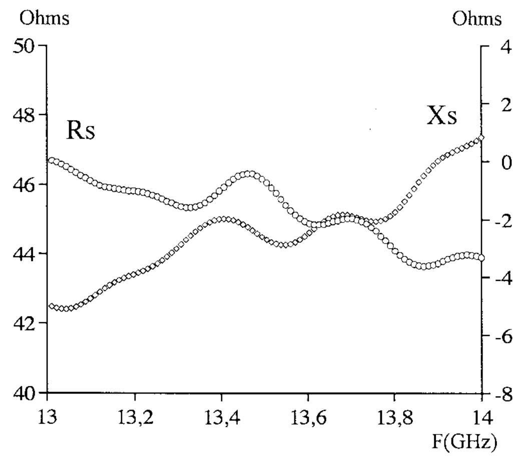

(b)

Fig. 4. Experimental curves of Rs and Xs of the Sierpinski carpet.

IV. Modeling

A. Principle

In order to foresee the behavior of a fractal copper film and, more particulary, to calculate its surface impedance, we propose to model the passage of a RPPW across our two samples and to calculate the expression for the electric field $\vec{E}$ and magnetic field $\vec{H}$ in the material. We will look for the solutions of plane wave type in the different zones.

The model considered is represented on the Fig. 6.

The association of zones one and two constitutes the fractal-structure copper film. Part one translates the metallic presence (ε_1, μ_0) while the part two translates the presence of a "hole" (ε_0, μ_0). Zone three represents the dielectric substrate (ε_2, μ_0) used as a support. Zones zero and four are made of air (ε_0, μ_0). "$\vec{k}_0$" is the wave vector oriented according to the z axis. The parameters a and b are, respectively, the thickness of the copper and the combined thickness of the metal and the dielectric substrate.

The RPPW reaches the fractal structure and then the part of the wave that has been neither reflected nor absorbed traverses the substrate. To this, add up the diffraction phenomena linked to the presence of holes. After having expressed the fields $\vec{E}$ and $\vec{H}$ in all the regions from the Maxwell's equations and having applied the conditions of continuity at the interfaces, a system of n equations with n unknowns is obtained. The value of n depends directly on the fractal structure under study. The resolution of such a system is carried out thanks to a mathematical software. The surface impedance if finally obtained from the following relation:

$$Zs = \frac{E_{\Sigma(z=0)}}{H_{\Sigma(z=0)}} \tag{2}$$

where $E_{\Sigma(z=0)}$ and $H_{\Sigma(z=0)}$ are, respectively, the sum of the tangential components of the fields $\vec{E}$ and $\vec{H}$ at the surface of the fractal film, i.e., at $z = 0$.

B. Fresnel Diffraction Applied to the Fractal Structures

The Fresnel's diffraction is applied when the condition of Fraunhofer is not satisfied [5]; that is

$$\frac{l^2 + L^2}{r\lambda} \ll 1$$

where (l, L) are the dimensions of the rectangular aperture and r the distance of the observation point from the plane of diffraction.

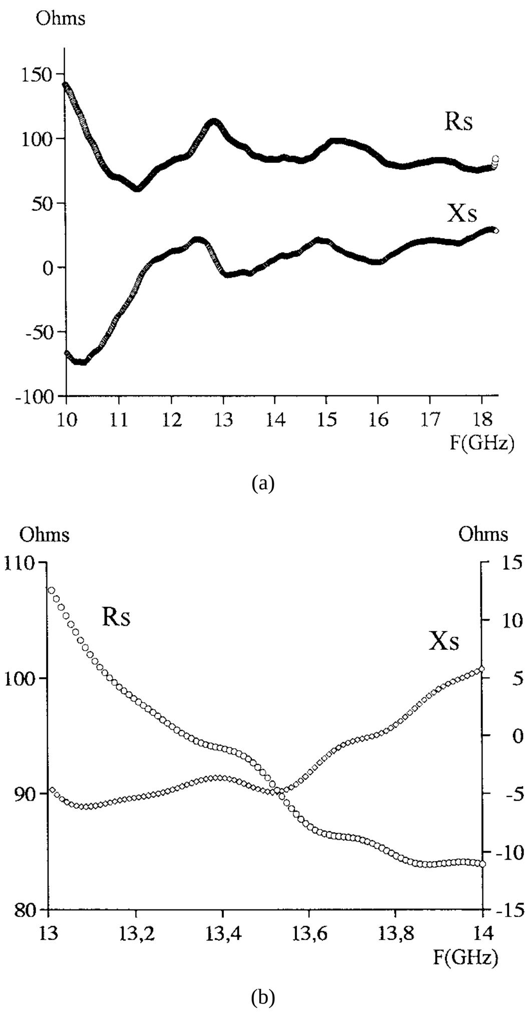

Fig. 5. Experimental curves of Rs and Xs of a Von Koch curve.

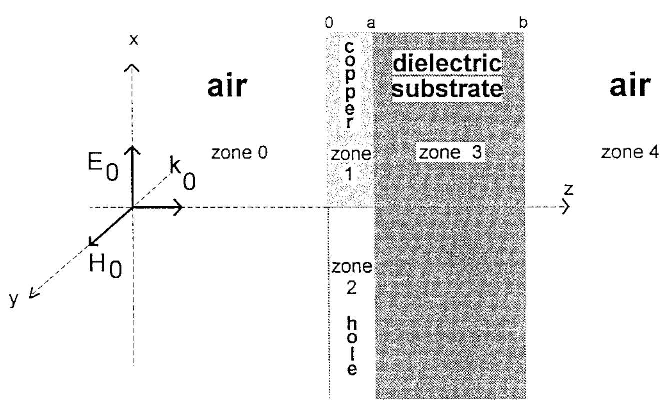

Fig. 6. Schematic representation of the propagation of the RPPW.

In our case, l and L vary from some centimeters to some millimeters for the two samples, r is of the order of 35 μm (copper thickness) and 1.5 cm $\leq \lambda \leq 3$ cm for a frequency range of 10–20 GHz. As such, the Fraunhofer condition is not verified.

We consider a homogeneous plane wave that falls following the normal to the surface of an indefinite plane screen perfectly

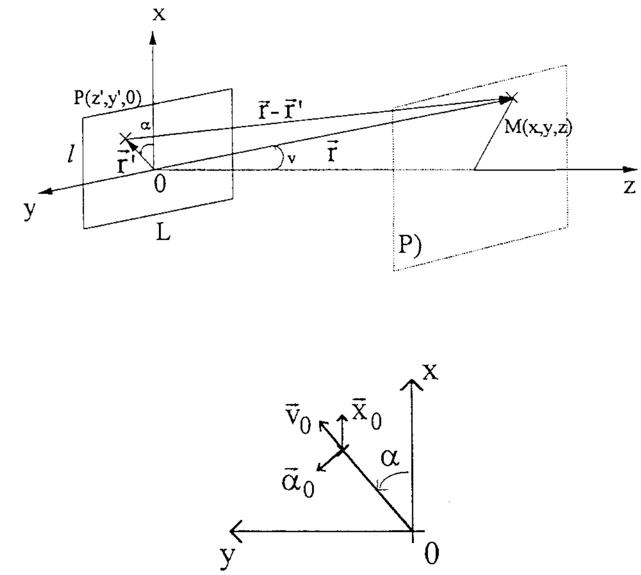

Fig. 7. Geometrical considerations.

conductor drilled with a hole (Fig. 7)

$$\vec{E}_0 = Z_0 H_0^+ e^{-jk_0 z} \vec{x} \tag{3}$$

$$\vec{H} = H_0^+ e^{-jk_0 z} \vec{y} \tag{4}$$

where $\vec{E}_0$ and $\vec{H}_0$ are, respectively, the incident electric and magnetic fields, H_0^+ is the modulus of the magnetic wave, and Z_0 the impedance of the vacuum.

The point of observation $M(x, y, z)$ belongs to a certain plane $z =$ constant (P) quite close to the rectangular aperture of dimensions $l \times L$. The resulting electric field at the point M is given by

$$\begin{aligned}\vec{E}_{\text{diff}} = {} & \frac{jZ_0 H_0^+ k_0}{4_\Pi |r - r'|}(1 + \cos v)(\vec{v}_0 \cos\alpha - \vec{\alpha}_0 \sin\alpha) \\ & \cdot \int_S \frac{e^{-jk_0|r-r'|}}{|r - r'|}\, dx'\, dy'\end{aligned} \tag{5}$$

the integral covering the diffracting surface.

Conserving the quadratic term of the limited development of $|r - r'|$, we obtain

$$\begin{aligned}|r - r'| &= \sqrt{(x - x')^2 + (y - y')^2 + z^2} \\ &= z + \frac{(x - x')^2 + (y - y')^2}{2z} + \cdots.\end{aligned}$$

Limiting our analysis to small values of angle v (i.e., taking position in the neighborhood of the z axis), it can be admitted that

$$|r - r'| \approx z^{-1} \quad \text{and}$$

$$(1 + \cos v)(\vec{v}_0 \cos\alpha - \vec{\alpha}_0 \sin\alpha) \approx 2\vec{x}_0.$$

Under these considerations, one obtains

$$\begin{aligned}\vec{E}_{\text{diff}}(z) = {} & \frac{jZ_0 H_0^+ k_0}{2_\Pi}; \frac{e^{-jk_0 z}}{z} \int_{-(l/2)}^{l/2} \int_{-(L/2)}^{L/2} \\ & \cdot e^{-jk_0((x-x')^2 + (y-y')^2/2z)}\, dx'\, dy'\, \vec{x}_0.\end{aligned} \tag{6}$$

The calculation of these two integrals of the same type is performed with the help of a change of variable. We put

$$\frac{k_0(x-x')^2}{2z} = t^2$$

which gives

$$\int_{-(l/2)}^{l/2} e^{-jk_0((x-x')^2/2z)}\,dx' = -\sqrt{\frac{2z}{k_0}}\int e^{-jt^2}\,dt.$$

We proceed in the same manner for the integral with respect to y'.

In this way, we have obtained the integrals (called Fresnel integrals) for which the conventional notations are the following:

$$\int_0^u e^{jt^2}\,dt = \int_0^u \cos t^2\,dt - j\int_0^u \sin t^2\,dt = \sqrt{\frac{\pi}{2}}[C(u) - jS(u)].$$

The functions $C(u)$ and $S(u)$, damped sinusoids tending toward 0.5, are given in the tables.

The expression of the electric field becomes

$$\vec{E}_{\text{diff}}(z) = \frac{jZ_0H_0^+}{2}e^{-jk_0z} \cdot [C(u) - jS(u)]_{u_1}^{u_2}[C(v) - jS(v)]_{v_1}^{v_2}\vec{x}_0$$

with

$$u_1 = \sqrt{\frac{k_0}{2z}}\left(x + \frac{1}{2}\right) \quad u_2 = \sqrt{\frac{k_0}{2z}}\left(x - \frac{1}{2}\right)$$

and

$$v_1 = \sqrt{\frac{k_0}{2z}}\left(y + \frac{L}{2}\right) \quad v_2 = \sqrt{\frac{k_0}{2z}}\left(y - \frac{L}{2}\right)$$

or

$$\vec{E}_{\text{diff}}(z) = \frac{jE_0(z)}{2} \cdot [C(u) - jS(u)]_{u_1}^{u_2}[C(v) - jS(v)]_{v_1}^{v_2}\vec{x}_0. \tag{7}$$

Following the same reasoning, we obtain the magnetic field

$$\vec{H}_{\text{diff}}(z) = \frac{jH_0(z)}{2} \cdot [C(u) - jS(u)]_{u_1}^{u_2}[C(v) - jS(v)]_{v_1}^{v_2}\vec{y}_0 \tag{8}$$

with

$$H_0(z) = \frac{E_0(z)}{Z_0} = H_0^+e^{-jk_0z}.$$

In order to simplify, the diffraction fields are considered only up to the observation point $M(0,0,z)$. This implies

$$u_{1,2}(z) = \pm\frac{\sqrt{\pi}}{2}\,\frac{l}{\sqrt{\lambda z}} \quad \text{and} \quad v_{1,2}(z) = \pm\frac{\sqrt{\pi}}{2}\,\frac{l}{\sqrt{\lambda z}}.$$

We note $\hat{l} = (l/\sqrt{\lambda z})$ and $\hat{L} = (L/\sqrt{\lambda z})$ the wave dimensions of the aperture.

For a square aperture (the most frequent case for our samples) the wave dimensions $\hat{l}$ and $\hat{L}$ are identical, i.e., $u_1 = v_1$ and $u_2 = v_2$. Hence

$$\vec{E}_{\text{diff}}(z) = \frac{jE_0(z)}{2}[[C(u) - jS(u)]_{u_1}^{u_2}]^2\vec{x}_0 \tag{9}$$

and

$$\vec{H}_{\text{diff}}(z) = \frac{jH_0(z)}{2}[[C(u) - jS(u)]_{u_1}^{u_2}]^2\vec{y}_0. \tag{10}$$

As an indication, one can easily verify that if in one hand $\hat{l} = \hat{L}$ and on the other $\hat{l} \gg 1$ (aperture very large compared to λ), the expressions of $\vec{E}$ and $\vec{H}$ are considerably simplified

$$\begin{aligned}\vec{E}_{\text{diff}}(z) &= Z_0H_0^+e^{-jk_0z}\vec{x}_0\\ &= \vec{E}_0 \ \text{ knowing that } \ C(-u) = -C(u)\\ \vec{H}_{\text{diff}}(z) &= H_0^+e^{-jk_0z}\vec{y}_0 = \vec{H}_0 \quad \text{and} \quad S(-u) = -S(u).\end{aligned}$$

We find in these conditions the expression of the incident wave which has not been distorted (3), (4).

C. Resolution of a System of Equations and Results

The route of the RPPW across the entire sample is translated by a set of equations issued from Maxwell's equations. The components of the fields $\vec{E}$ and $\vec{H}$ are expressed as function of z in each zone of the Fig. 6 according to whether to incident wave has encountered a hole or a copper film. Applying the conditions of continuity to the interfaces, one obtains a system of n equations with n unknowns

- in $z = 0$ copper
$$\begin{cases}(H^+)0 + H_0^-) - (H_1^+ + H_1^+) = 0\\ Z_0(H_0^+ + H_0^-) - j\dfrac{k_1}{\sigma_1}(H_1^+ + H_1^-) = 0\end{cases}$$

- in $z = a$ copper
$$\begin{cases}(H_1^+e^{-jk_1a} + H_1^-e^{+jk_1a}) - (H_2^+e^{-jk_2a} + H_2^-e^{+jk_2a}) = 0\\ j\dfrac{k_1}{\sigma_1}(H_1^+e^{-jk_1a} - H_1^-e^{+jk_1a}) - Z_2(H_2^+e^{-jk_2a} - H_2^-e^{+jk_2a}) = 0\end{cases}$$

hole α
$$\begin{cases}\left(\dfrac{H_0^+}{2}e^{-jk_0a}[[C(u) - jS(u)_{u_1}^{u_2}]^2 + H_0^{\alpha-}\right) - (H_2^{\alpha+}e^{-jk_2a} + H_2^{\alpha-}e^{+jk_2a}) = 0\\ Z_0\left(j\dfrac{H_0^+}{2}e^{-jk_0a}[[C(u) - jS(u)_{u_1}^{u_2}]^2 - H_0^{\alpha-}\right) - Z_2(H_2^{\alpha+}e^{-jk_2a} - H_2^{\alpha-}e^{+jk_2a}) = 0\end{cases}$$

- in $z = b$ copper
$$\begin{cases}H_2^+e^{-jk_2b} + H_2^-e^{+jk_2b} - H_3^+e^{-jk_0b} = 0\\ Z_2(H_2^+e^{-jk_2b} - H_2^-e^{+jk_2b} - Z_0H_3^+e^{-jk_0b} = 0\end{cases}$$

hole α
$$\begin{cases}(H_2^{\alpha+}e^{-jk_2b} + H_2^{\alpha-}e^{+jk_2b}) - H_3^{\alpha+}e^{-jk_0b} = 0\\ Z_2(H_2^{\alpha+}e^{-jk_2b} - H_2^{\alpha-}e^{+jk_2b}) - Z_0H_3^{\alpha+}e^{-jk_0b} = 0.\end{cases}$$

Following is an explanation of the parameters:

- the index gives the concerned zones (Fig. 6: zone 0—air; zone 1—copper; etc.);
- the exponents "+" and "−" indicate, respectively, that the wave is incident or reflected;
- the exponent "α" indicates the diffractant aperture to which these equations are related.

In $z = a$ and $z = b$, there are as many pairs of equations outside copper as there are different holes. It leads to a system of 22 equations with 22 unknowns for the Sierpinski carpet, and of 30 equations with 30 unknowns for the curve of Koch (respectively, four and six different apertures). The resolution is done as function of the amplitude of the incident wave H_0^+.

An elementary cell of the sample associated with H_0^+ is designated, then the set of fields $\vec{E}$ are added up and $\vec{H}$ listed at the surface of the fractal film taking into account—on one hand, the number of "full" cells (copper) and on the other hand, the size of the "empty" cells (diffractant apertures) and their surface area. This way one obtains $E_{\Sigma 0}$ as functions of $H_{\Sigma 0}$ and, according to (2), the surface impedance Z_s.

The results of this modeling are shown on the Figs. 8 and 9 with on one hand, the curves over the range (10 GHz, 20 GHz), and on the other hand, an enlargement on the interval [13 GHz, 14 GHz].

In both cases, the order of magnitude of Rs and Xs is satisfactory. Each time, the principle oscillation is well reproduced by the simulation. Moreover, it is observed on the theoretical curves that a high number of oscillations of diverse frequencies are also discerned on the experimental results. Nevrtheless, amplitudes of experimental curves look to be weaker, certainly because of a too large attenuation of the electromagnetic wave. Taking into account the frequency domain under consideration, the substrate generates losses cannot be neglected. So, we have chosen to introduce into the theoretical calculations a value of the dielectric permittivity containing a loss angle. We have finally opted for $\varepsilon_{r2} = 3.1e^{-j0.6}$.

An extension of the range [1 GHz, 80 GHz] of the simulation of the two samples (Fig. 10) provides curves with one principal oscillation on which are transplanted other oscillations of diverse frequencies and small amplitudes. The frequency and the amplitude of each main oscillation are closely correlated to the characteristics of the dielectric substrate. Indeed, the frequency band ΔF (ΔF: frequency band on which is extended one period of the oscillation under consideration) tends to decrease with the increase (on one hand) of the thickness of the substrate and (on the other hand) of the dielectric losses. In addition, the more or less perfect character of the dielectric acts also on the principal amplitude. Taking into account the small size of the experimental observation window compared to the simulation range [1 GHz, 80 GHz], the smallest variation of ε_{r2} generates a different slope on the theoretical behavior over the range [10 GHz, 20 GHz]. That is why the difference between the slopes is not fundamental as linked to the dielectric substrate. One can note (with identical supports) that the ratio of the average value of the two theoretical curves Rs (Fig. 10: $\langle Rs\rangle_{\mathrm{Koch}} \approx 160\ \Omega$

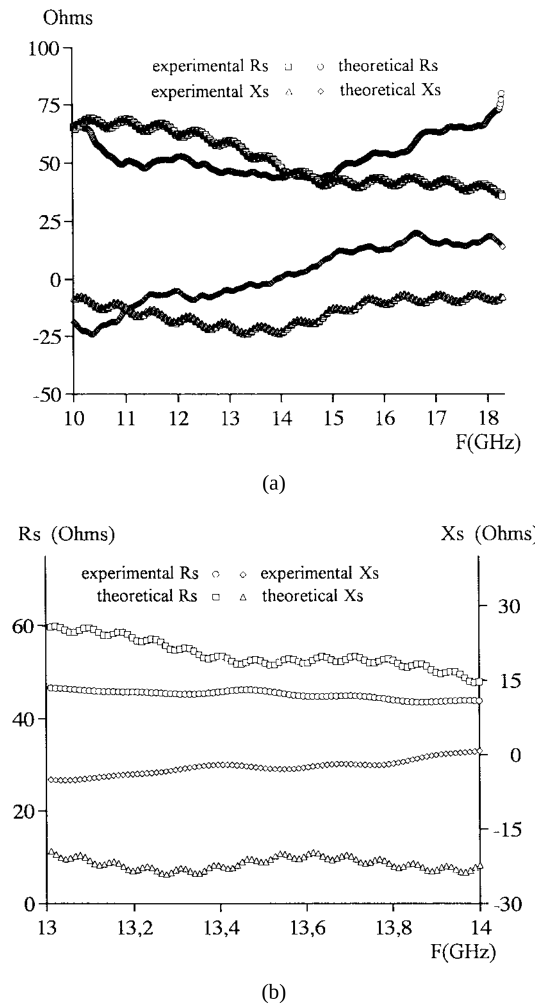

Fig. 8. Experimental and theoretical curves of Rs and Xs of the Sierpinski carpet.

and $\langle Rs\rangle_{\mathrm{Sierpinski}} \approx 55\ \Omega$) is equivalent to the inverse ratio of the copper contents in the two structures equal to approximately "2.9." The multiple small oscillations result from the accumulated effects of each diffractant aperture. The Table II explains that to each hole of known area, an oscillation can be observed on the theoretical curves (Figs. 8–10). Indeed, we find

$$\frac{\Delta F_i}{\Delta F_j} = \frac{S_j}{S_i}$$

where ΔF_i and S_i represent, respectively, the frequency band of the oscillation i and the area of the diffractant surface i.

The developed expression of Zs has an overall imaginary part proportional to the size and the number of each diffractant aperture. For the Sierpinski carpet, whose each hole of a different size squares with a new iteration, we can deduce from the theoretical curves Xs the following relation:

$$Df = \frac{\ln\left(\dfrac{\Delta A_i}{\Delta A_{i+1}}\right)^2}{\ln\left(\dfrac{\Delta F_i}{\Delta F_{i+1}}\right)^{1/2}}$$

TABLE II
DIFFRACTANT APERTURES AREA AND FREQUENCY BANDS ΔF OBSERVED ON THE THEORETICAL CURVES

	Area of the holes(cm^2)	Sj / Si		ΔF(GHz)	ΔFi / ΔFj	
Substrate	---	---	---	60	---	---
Sierpinski carpet	S_1=14.88 10^{-3}	S_2/S_1=9		ΔF_1=55.4	$\Delta F_1/\Delta F_2$=9	
	S_2=0.135	S_3/S_2=9		ΔF_2=6.16	$\Delta F_2/\Delta F_3$=9.1	
	S_3=1.21	S_4/S_3=9		ΔF_3=0.68	$\Delta F_3/\Delta F_4$=8.8	
	S_4=10.89			ΔF_4=0.08		
Von Koch curve	S_1=82.4 10^{-3}	S_2/S_1=5.12		ΔF_1=10	$\Delta F_1/\Delta F_2$=5.1	
	S_2=0.422	S_3/S_2=1.54		ΔF_2=1.9	$\Delta F_2/\Delta F_3$=1.5	
	S_3=0.65	S_4/S_3=1.54	S_5/S_1=49	ΔF_3=1.24	$\Delta F_3/\Delta F_4$=1.5	$\Delta F_1/\Delta F_5$ =50
	S_4=1	S_5/S_4=4.04		ΔF_4=0.8	$\Delta F_4/\Delta F_5$=4	
	S_5=4.04	S_6/S_5=2.47		ΔF_5=0.2	$\Delta F_5/\Delta F_6$=2.5	
	S_6=10			ΔF_6=0.08		

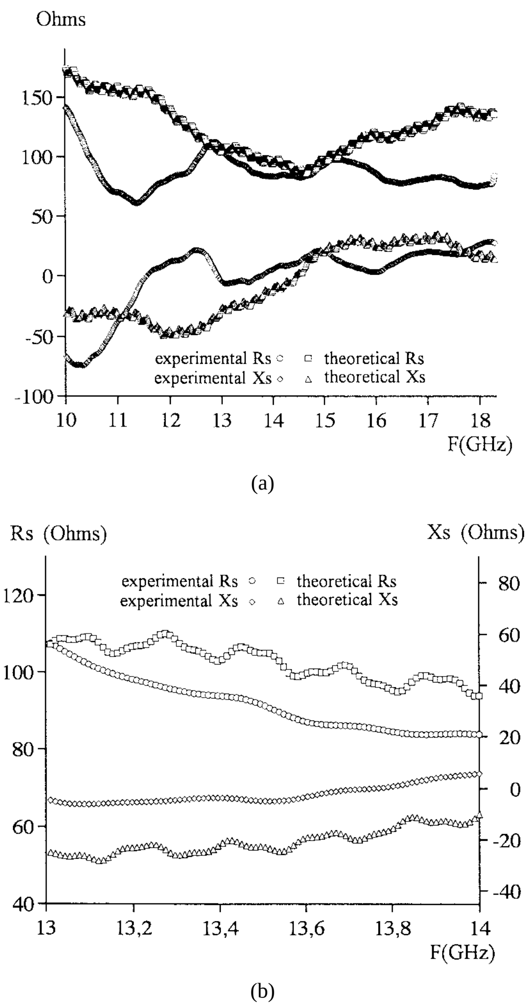

Fig. 9. Experimental and theoretical curves of Rs and Xs of a Von Koch curve.

where Df is the fractal dimension, ΔA_i and ΔF_i, respectively, the amplitude and the frequency band ΔF of the oscillation i, and the $(i+1)$ level the first oscillation that is superimposed on the level i [Fig. 10(a)]. This relation is a characteristic of the fractal geometry as opposed to Euclidean structures.

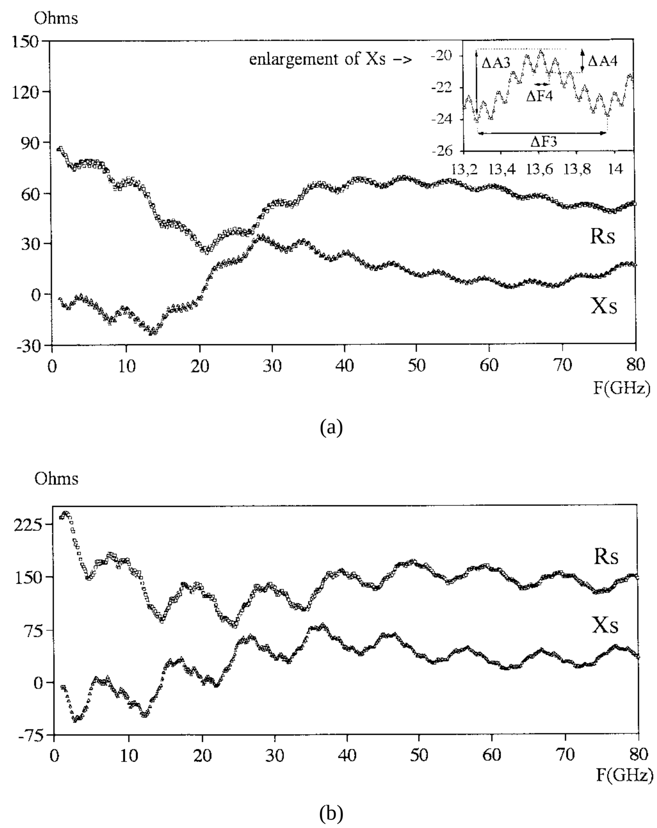

Fig. 10. Simulation of Rs and Xs of the two samples for a frequency included between 1 and 80 GHz.

We can also verify that the smaller apertures generate the most important secondary oscillations. Moreover, all the oscillations damp down with the increase of the frequency—the wavelength becoming very short beside the holes' size.

V. CONCLUSION

We have measured, in free-space, the surface impedance of the copper films of fractal structure having fractal dimensions $D = 1.89$ and $D = 1.5$. The proposed modeling from Maxwell's equations (locally applied) and Fresnel's diffraction (generalized to the set of the diffractant apertures) gives an overall interpretation of the phenomena experimentally observed within the range [10 GHz, 20 GHz]. It also appears that, for a structure which the process of iteration is easy, the real and imaginary part of the surface impedance take account of the fractal nature. In fact, this innovating result was expected thanks to the modeling that describes accurately the process of iteration. So, the number and the size of each apertures as well as the scale law are included in the final relation of the surface impedance Z_S; that is, the reason we supposed the curves were containing the information about fractal dimension. Thus, we have put in evidence the existence of a particular scale law in the impedance behavior linked to fractal aspect. Our problem consists now in confirming from the equations the relation graphically determined. At last, for our two samples, the average value of the signal is directly linked to the quantity of copper in the surface and the oscillations result from the superposition of all the effects due to the diffraction.

REFERENCES

[1] B. B. Mandelbrot, *Fractals, Form, Chance and Dimension*. San Francisco, CA: Freeman, 1977.

[2] J. Feder, E. Hinrichsen, K. J. Måløy and T. Jøssang, *Physica D*, vol. 38, p. 104, 1989.

[3] J.-F. Gouyet, *Physique et Structures Fractales*. Paris, France: Masson, 1992.

[4] Centre d'Etudes et de Recherches de Toulouse2, Toulouse, 31400 France.

[5] V. Nikolski, *Electrodynamique et Propagation des Ondes Radioélectriques*. Moscow, Russia: Mir, 1972.

Emmanuel Troncet received the Ph.D. degree in electronics from the Paul Sabatier University, Toulouse, France, in 1997.

His research interest is in elaboration and electrical analysis of fractal structures. He is a member of the research team at the Paul Sabatier University, Toulouse, France.

Guy Ablart received the Ph.D. degree in electronics from the Paul Sabatier University, Toulouse, France, in 1978.

He is a Professor of electronics and microwave propagation at the Paul Sabatier University, Toulouse, France. His research interest is in the elaboration and the electrical characterization of fractal structures and analysis of their microwave response.

Levi Allam received the Ph.D. degree in electronics from the Paul Sabatier University, Toulouse, France, in 1988.

He is a Professor at the Chartres Institute of Technology, France, where he teaches electronics and electrical engineering. His research interest is in the geometrical analyzes of random fractal structures.